ELSEVIER

www.elsevier.nl/locate/carres

Carbohydrate Research 330 (2001) 249–256

CARBOHYDRATE RESEARCH

Internal structure of the starch granule revealed by AFM

Andrew A. Baker,[a] Mervyn J. Miles,[a,*] William Helbert [b]

[a]*H.H. Wills Physics Laboratory, University of Bristol, Tyndall Avenue, Bristol BS8 1TL, UK*
[b]*Station Biologique, Centre National de la Recherche Scientifique, Unité Mixte de Recherche CNRS/Laboratoires Goëmar S.A. (U.M.R. 1931), BP 74, F-29682 Roscoff, France*

Received 27 June 2000; received in revised form 26 September 2000; accepted 18 October 2000

Abstract

Atomic force microscopy images of sectioned native corn starch granules show evidence of the well-known radial organisation of the starch macromolecules, with the less-ordered hilum region near to the centre. Native granules show blocks 400–500 nm in size that span the growth rings. Lintnerised starch granules, where a mild acid hydrolysis has been used to remove the amorphous and less crystalline parts of the granule, clearly show smaller 'blocklets' within the rings approximately 10–30 nm in size. This level of organisation within the growth rings corresponds to the blocklet or superhelix structures that have been proposed in the literature for the association or clustering of amylopectin helices. Mechanical property imaging techniques have provided enhanced contrast to view this morphology, and shown the deformability of the starch structure under contact mode imaging conditions.

Keywords: Starch structure; Blocklet; AFM; High-resolution; Tapping mode; Phase imaging; Force modulation; Lateral force microscopy; Mechanical properties

1. Introduction

The structure of starch granules has been categorised using physical techniques at several morphological levels. Our knowledge of granule organisation up to the mid-1980s was comprehensibly reviewed by French,[1] and has been supplemented by more recent articles.[2,3] Growth rings are often seen in granules, and the two macromolecules, amylopectin and amylose, are arranged radially with their molecular axes aligned perpendicular to the growth rings and to the granule surface. The growth rings themselves may be broken into smaller 'blocklets' due to the creation of radial canals on swelling that break up the rings. This definition of a blocklet, due to Badenhuizen, is for structures that are visible optically with a size of approximately 1 μm, and these are artifacts due to the separation of layers rather than preformed structures.[4] Smaller 'clumps' have been seen in electron microscopic studies of starch sections, with a width of 100–150 nm and a length of 300–500 nm.[4,5] At an even smaller scale, 'microgranules' of 20–30 nm have been observed,[4–6] and at the finest level of detail seen under the transmission electron microscope, thin sections of acid treated granules show stacks of crystalline lamellae 5 nm thick approximately parallel to the growth rings.[7] Small angle X-

* Corresponding author. Tel.: +44-117-9288707; fax: +44-117-9255624.
E-mail addresses: andy.baker@bristol.ac.uk (A.A. Baker), m.j.miles@bristol.ac.uk (M.J. Miles).

0008-6215/01/$ - see front matter
PII: S0008-6215(00)00275-5

ray scattering in starch from many different species has revealed a consistent 9 nm periodicity due to the combined size of crystalline plus amorphous lamellae species.[8]

The blocklet concept was revived more recently by Gallant et al.[9] to describe the organisation of amylopectin lamellae into effectively spherical blocklets, with diameters from 20 to 500 nm depending on the botanic origin of the starch and their location within the granule. SEM studies of wheat starch found small blocklets approximately 25 nm in size in the semi-crystalline shells, and larger 80–120 nm blocklets in the hard crystalline layers. Potato starch shows much larger blocklets of 200–500 nm.

Atomic force microscopy (AFM) has been previously used to examine starch structure, although there are few publications and they have been concerned with the exterior surface of the starch granule.[9–14] On wheat starch, small protrusions of 10–50 nm were observed, whereas larger spherical protrusions (200–500 nm) were seen on the surface of native potatoe starch granules.[9,13,14] These dimensions are consistent with the idea that the surface protrusions and blocklets within the granule are the same structures.

In this paper, AFM has been used to examine the interior surface of granules, which have been embedded in melamine resin and microtomed into ultra-thin sections. Studies of such sections by TEM were mostly done several decades ago,[5,7,15–18] and involved complex multi-step preparation techniques that included either metal shadowing or staining, although more recent low-dose electron microscopy has not required these steps.[19] No such preparations are necessary for AFM investigations, and therefore artifacts from these treatments are eliminated. Significant averaging of the structure occurs by passing electrons or X-rays through a sample of finite thickness, even with electron[19,20] or synchrotron radiation[21,22] probe sizes of the order of 1 μm in diameter. AFM is superior in this respect, as it offers the advantage of highly localised ($\sim$ nm) topographic imaging, as well as qualitative material property imaging for non-topographic insights into granule structure.

2. Results and discussion

Fig. 1 shows tapping mode topographic and phase images of ~ 100 nm thick sections of corn starch embedded in Nanoplast resin. Most, but not all, images in Fig. 1 from native granules show no indication of the ring structure, consistent with early electron microscopic observations of sections through maize endosperm where less than 15% of the starch granules showed growth rings.[4,16] The most obvious topographic features are arranged in a radial fashion like the spokes of a wheel. These 'spokes' are a preparation artifact due to compression and folding of the starch during the collection of the sections on water.[17,23] When one side of the flat, newly-cut section comes into contact with the surface of the water in the collecting tank, it swells and bows into a hemi-spherical shape. The stresses generated in the swollen granule section cause it to buckle and then finally to form 'S-shaped' folds. In transmission electron micrographs these folds appear dark due to the reduced electron flux through these areas.[23]

The unique ability of the AFM to measure topography at the nanometre scale shows that the remaining flat parts of the granule are at the same height (< 5 nm difference) as the surrounding resin. The moduli of the starch and resin are similar, since where they are sharply different the cutting knife deforms one component more than the other resulting in a poor interface between specimen and matrix. The phase image in Fig. 1(b) is nevertheless sensitive to subtle differences in the mechanical or surface properties of the granule and the surrounding resin, as the granule sections are lighter in colour than the surrounding matrix. The colour variation indicates a difference in phase angle lag between the sinusoid driving the cantilever and the detected cantilever oscillation, owing to energy loss when the probe interacts with the surface.[24,25] Precise interpretation of the differences is a beyond the scope of this study, and this complicated issue is made worse by conflicting reports in the literature.[26] The contrast between the Nanoplast resin and starch will be due to a combination of differences in modulus or tip-sample adhesion, possibly due to local variations in surface hydration.[27]

There is also variation in the phase signal within a particular granule section. Moving from the periphery to the centre, the image often appears to get slightly brighter. The brighter regions also coincide with an increase in the surface corrugation due to the pleating, which can be seen by comparing the phase image with the topographic image in (b). Permanent strain introduced into different parts of the granule by the folding stresses during hydration may lead to modulus variations and consequently phase angle shifts.

Detailed evidence of the radial organisation of starch granules is shown in Fig. 2. In several of the images, there is a 'rippled' appearance outside the area of the starch granule. This is presumably caused by microtome knife 'chatter' during preparation, although it is interesting to note the sharp boundary with the granule, which appears not to have suffered from this motion. This suggests a plastic deformation of the resin, whilst any deformation of the starch which may have occurred was reversible.

The raised centre in Fig. 2(a) has finger-like protrusions running out towards the edge of the granule for several microns. The deflection image in (b) also highlights these features. Close to the less-ordered structure of the hilum in the centre, the width of the radial features is much larger and ~ 1 μm. These are cracks caused by swelling in water and subsequent drying.[4] These observations support the currently accepted model of the starch granule architecture where the molecular chains of starch are more or less perpendicular to the growth rings and to the surface of the granule.[7]

Towards the outer edge of the section in Fig. 2(a), there are growth rings spaced by ~ 450 nm, and in (c) there are slightly finer rings with widths of ~ 100–200 nm. Both of these ring sizes are well within the normal range of 150–700 nm observed for corn starch.[18] The formation of distinct rings results from both the apposition of new material on the granule and the action of swelling, with the largest rings towards the outer edge of the granule where the swelling is greatest.

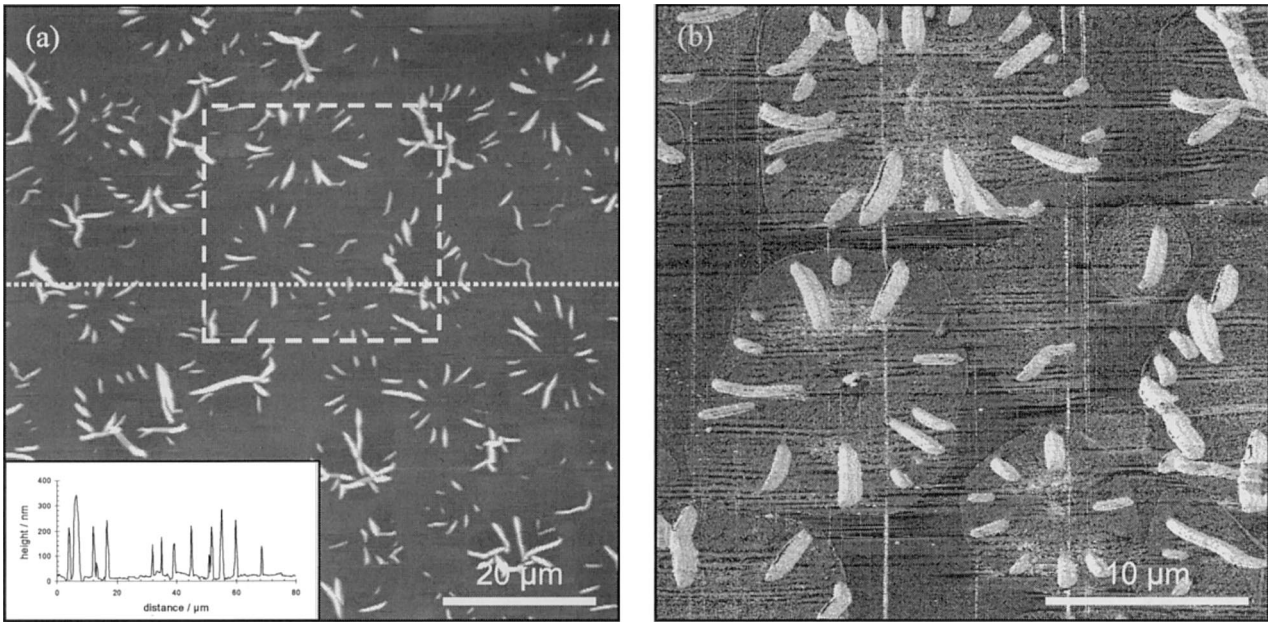

Fig. 1. Low magnification tapping mode images of a typical field of sections through embedded starch granules. (a) Topographic image containing ~ 50 individual sections. The near-radial 'spokes' are due to swelling and folding of the starch during preparation and collection on water. The inset graph shows a line section taken across the image at the location of the dotted white line, showing that the folds protrude ~ 150–300 nm above the background. (b) Shows a phase image of the sections from the region indicated in (a). Although the topographic difference between the sections and their surrounding area is typically < 5 nm, the starch granules and the surrounding resin are clearly delineated due to the different mechanical properties of the starch and resin causing phase angle shifts. The vertical lines are scores due to imperfections in the cutting knife, whilst the 'pleats' running across the image are due to folding during preparation.

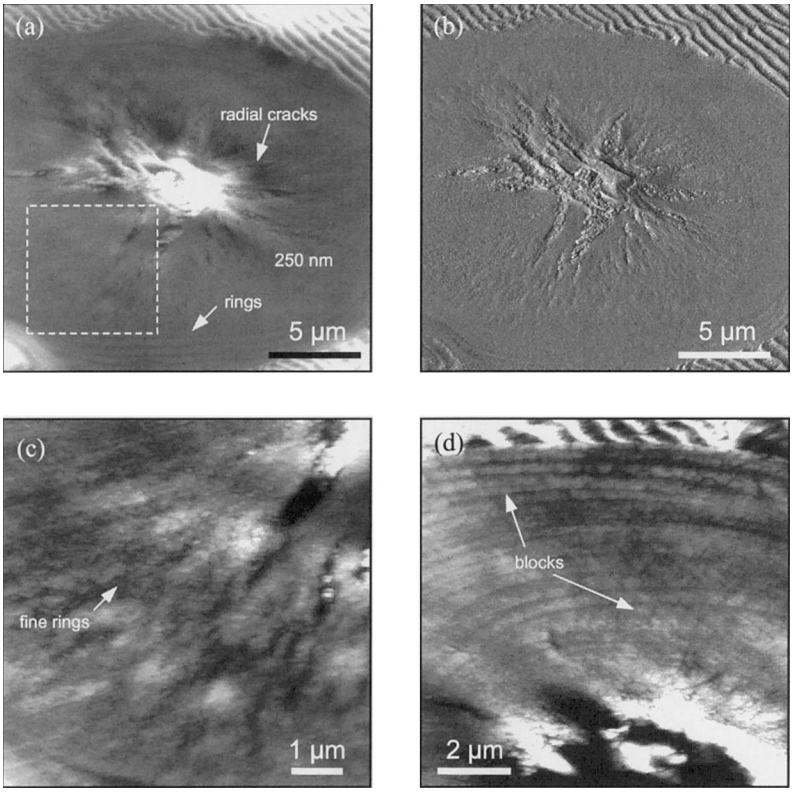

Fig. 2. Contact mode images showing central sections revealing detail near to the granule hilum. In the topographic image shown in (a), the raised centre has radial cracks which get narrower further away from the centre. Distinct rings can be seen at the periphery of the section with a spacing ~450 nm. (b) Shows the corresponding deflection (error-signal) image. The area indicated by the box is enlarged in (c). Finer rings can also be distinguished, slightly closer together than the outermost rings. In (d) small blocks spanning the growth rings ~400–500 nm in size are visible.

In contrast to the cracks in Fig. 2(a)–(c), fine radial lines rather than larger cracks are present in the image shown in (d) from a different granule. The centre of the granule towards the bottom of the image in Fig. 2(d) is depressed where parts of the hilum have been pulled out completely by the cutting action of the knife. The maximum depth of the hole is ~90 nm, comparable with the thickness of these sections. Larger blocks measuring 400–500 nm across span the growth rings. The sample preparation method does not allow us to determine if this is a natural feature of the granule, or whether swelling during hydration has caused it. In either case, there must be structural weakness between the blocks for their formation to occur.

Fig. 3 shows low magnification images of a sample of lintnerised starch. The acidic hydrolysis of the amylopectin branch points leaves mainly linear oligosaccharides, and reduces the swelling ability of the granules such that the folds shown in Fig. 1 are not produced.[4] Some of the granules shown in Fig. 3 have narrow rings at the edge that widen as the centre of the section is approached, owing to the position of the cutting. The apparent thickness of the ring depends on whether the position of the cross-section is central or non-central.[7]

One of the innovative contributions of AFM to starch research is illustrated by the three pairs of topographic and 'mechanical property' images shown in Fig. 4. The topographic images all clearly show the growth rings, but these are less clearly visible in their associated mechanical property images. The comparative appearance of the granules when imaged by the three separate techniques demonstrates the interesting and novel information that scanning probe techniques provide. Fig. 4(b) shows a tapping mode phase image, where the isolated features are in the range of 10–30 nm across. The phase image resolves blocklets an order of magnitude smaller than the features shown in Fig.

2(d), suggesting that they are a distinct morphology, and it is features on this scale (in corn starch) that appear to be aptly described as blocklets. The smallest blocklets seen may correspond to structures such as the amylopectin superhelices found in potato starch.[28,29] In this model, each superhelix has an outer diameter of 18 nm, close to the sizes reported here. Larger features in these images could be due to clustering of superhelices. Other arrangements of the individual amylopectin helices are also possible, although it has not been possible to resolve details at this level in the present study. Interpreting phase images and extracting quantitative information is very difficult,[24,25] but the technique is useful in providing sharp contrast between, for example, amorphous and semi-crystalline material in polymers,[30,31] The sharp contrast seen here may be due to differences in the distribution of water over the surface,[27,32] although further experiments would be needed to confirm this.

Fig. 4(c) and (d) shows a force modulation amplitude image from the same starch granule section seen in (a) and (b). The topographic image in (c) is also less well resolved than the topographic image in (a). The amplitude image has striking features approximately two to three times larger than those in (b), clearly due to the same surface features as in (b), since the image is taken on precisely the same granule. The increased force exerted on the sample by the probe in this contact mode technique is most likely causing some deformation of the sample. Thus starch, which still consists of approximately 20% water even in its 'dry' form, is a deformable specimen under the influence of the imaging probe. The geometry of the AFM tips used for the two sets of images is slightly different and this may to a lesser extent contribute to variations in the precise dimensions observed. The contribution of the tip shape, which typically leads to features appearing to be enlarged laterally, must be kept in mind when making comparisons with other microscopic techniques.

In Fig. 4(e) and (f), lateral force microscopy images of the granule surface show the rings in the topographic image, but just as with the other mechanical property images, the ring structure is barely visible in the friction image. The circular features in (f) are dark, although reversing the scan direction caused a contrast reversal, as expected from a lateral force image showing true frictional contrast. It is unlikely that surface topography plays a significant part in the friction image contrast, or it would be expected that the growth rings, clearly visible in (e), would be strongly delineated in the friction image. The sizes of the features in the friction image are also slightly greater than those shown in (b) since, along with force modulation imaging, this is a contact mode technique.

Mechanical property imaging is an excellent means of enhancing contrast of features on the surface, and shows variations in material

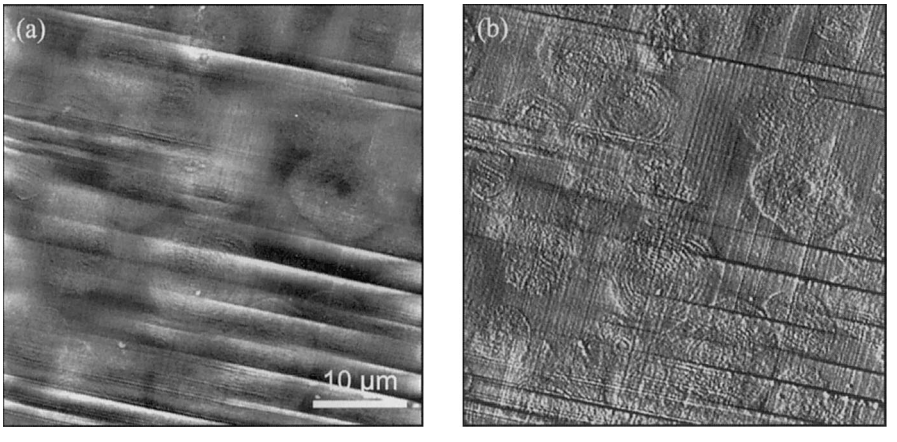

Fig. 3. Low magnification contact mode images of lintnerised starch sections. (a) and (b) show topographic and deflection (error-signal) images, respectively, where many starch sections can be seen without the folds seen in the native starch sections in Fig. 1. The growth ring structure of the granule is also clearly evident in most sections. Pleats formed during microtoming and faint knife cutting marks can again been seen.

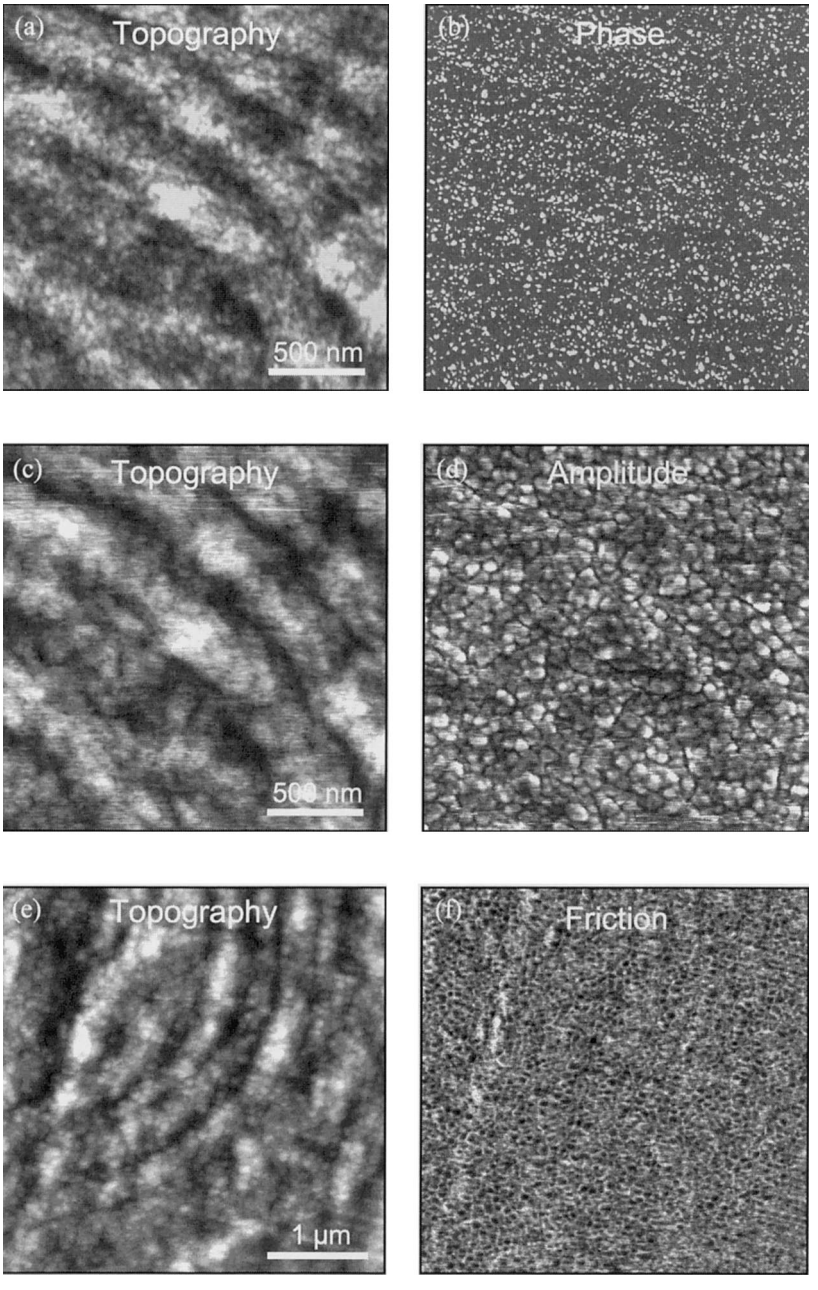

Fig. 4. Mechanical property imaging of lintnerised starch granule sections. (a) and (b) are tapping mode topographic and phase images, respectively. In the phase image, blocklet features 10–30 nm in size can be seen. (c) and (d) are force modulation topographic and amplitude images, respectively, from the same area shown in (a) and (b). In the amplitude image, the same blocket features appear larger due to the compression of the starch. (e) and (f) are LFM topographic and friction images, respectively, where blocklet structure is again evident.

or chemical properties across a specimen. Quantitative information is also in principle obtainable. Future investigations of mechanical property changes during manipulation of granule structure, for example under different humidity conditions or during gelatinisation, may provide interesting insights into the detailed structural changes occurring during these processes.

3. Experimental

Sample preparation.—Corn starch granules (Sigma) were embedded in Nanoplast™ resin (Agar Scientific). Aqueous melamine resin 10 g MME7002 were activated by 0.15 g of acid catalyst B52, and 0.1 ml of the Nanoplast resin was poured into an embedding mould. After curing for one night at 40 °C, concen-

trated dispersion of starch in water were mixed with Nanoplast and deposited onto the pre-hardened block bottom. These preparations were then cured for two days at 40 °C, followed by two days at 60 °C. The block was positioned on the specimen holder of a Reichert Ultracut-E microtome. It was first trimmed with glass knives and sectioned with a 45° Diatome diamond knife. The knife was set with a clearance angle of 6°. Thin sections 80–100 nm were obtained at a speed of 1 mm/s. The sections were collected with a platinum double loop (Chatani Ltd, Tokyo) and then deposited onto the surface of freshly-cleaved mica. Samples were stored in a Petri dish prior to examination by AFM. The partially lintnerised starch samples used in this study were obtained by subjecting the granule suspension to a mild acid hydrolysis treatment with 2.5 N HCl at 30 °C for 5 days. The suspension was neutralised by centrifuging several times in distilled water. Lintnerised starch was embedded without drying.

Atomic force microscopy.—AFM images were taken in air using a Digital Instruments (Santa Barbara, CA) NanoScope system with a MultiMode head. A 'J-scanner' with a range of ~ 140 μm, or a 'K-scanner' with a range of ~ 250 μm was used. Contact mode imaging used standard 200 μm long and 20 μm wide silicon nitride cantilevers with a nominal spring constant of 0.06 Nm^{-1}. Topographic and deflection, or error-signal, images were recorded. The error-signal images enhance high spatial frequencies on the specimen surface and offer improved contrast for sharper features. Tapping mode images were taken using standard commercial silicon cantilevers with a length of 125 μm. The cantilever was tuned to oscillate at, or slightly below, its resonance frequency (approximately 250–400 kHz). Force modulation images were obtained by applying a relatively low frequency oscillation to a silicon nitride cantilever, and recording the amplitude of the cantilever response. The amplitude changes in this dynamic contact mode technique depend on the mechanical properties of the sample. The 23.3 kHz oscillation frequency used is above the bandwidth of the feedback loop, so the applied imaging force deviates slightly from the mean 'constant force' operating position. For this reason, the smallest oscillation amplitudes that still provided adequate contrast were used. Lateral force microscopy was performed with the fast-scan direction perpendicular to the cantilever long-axis to introduce torsional modes of the cantilever deflection, which are sensitive to changes in tip-sample friction. Friction images were collected in both the 'trace' and 'retrace' directions to verify that contrast reversal was occurring as the scan direction changed. In all the imaging modes used in this study, some topographic information may couple into the mechanical property images if the constant force (contact mode) or constant amplitude (tapping mode) conditions are deviated from. This will only occur where the topographic features contain high spatial frequency components along the cantilever fast-scan direction.

Acknowledgements

We thank Dr Klaus Jandt (Department of Oral and Dental Science, University of Bristol) for the use of his MultiMode microscope to obtain some of the images presented here, and Professor Peter Shewry and Dr Arthur Tatham (IACR-Long Ashton) for helpful discussions and financial support.

References

1. French, D. In *Starch Chemistry and Technology*; Whistler, R. L.; Bemiller, J. N.; Paschall, E. F., Eds. Organization of Starch Granules. Academic Press: New York, 1984; 2nd ed. pp. 183–247.
2. T. Galliard, Ed., *Starch: Properties and Potential*, John Wiley, 1987.
3. Buléon, A.; Colonna, P.; Planchot, V.; Ball, S. *Int. J. Biol. Macromol.* **1998**, *23*, 85–112.
4. Badenhuizen, N. P. *Chemistry and Biology of the Starch Granule*; Springer: Berlin, 1959; Vol. 2.
5. Whistler, R. L.; Turner, E. S. *J. Polym. Sci.* **1955**, *18*, 153–156.
6. Z. Nikuni, S. Hizukuri, Structure of starch granules, In Memoirs of the Institute of Scientific and Industrial Research, Osaka University, 1957, 14, 173–181.
7. Yamaguchi, M.; Kainuma, K.; French, D. *J. Ultrastruct. Res.* **1979**, *69*, 249–261.
8. Jenkins, P. J.; Cameron, R. E.; Donald, A. M. *Starch/Stärke* **1993**, *45*, 417–420.
9. Gallant, D. J.; Bouchet, B.; Baldwin, P. M. *Carbohydr. Polym.* **1997**, *32*, 177–191.

10. A.A. Baker, PhD thesis, University of Bristol, 1998.
11. Thomson, N. H.; Miles, M. J.; Ring, S. G.; Shewry, P. R.; Tatham, A. S. *J. Vac. Sci. Technol. B* **1994**, *12*, 1565–1568.
12. N.H. Thomson, PhD thesis, University of Bristol, 1994.
13. Baldwin, P. M.; Frazier, R. A.; Adler, J.; Glasbey, T. O.; Keane, M. P.; Roberts, C. J.; Tendler, S. J. B.; Davies, M. C.; Melia, C. D. *J. Microsc.* **1996**, *184*, 75–80.
14. Baldwin, P. M.; Davies, M. C.; Melia, C. D. *Int. J. Biol. Macromol.* **1997**, *21*, 103–107.
15. Whistler, R. L.; Byrd, J. D.; Thornburg, W. L. *Biochim. Biophys. Acta* **1955**, *18*, 146–147.
16. Whistler, R. L.; Thornburg, W. L. *Agri. Food Chem.* **1957**, *5*, 203–207.
17. Buttrose, M. S. *J. Ultrastruct. Res.* **1960**, *4*, 231–257.
18. Mussulman, W. C.; Wagoner, J. A. *Cereal Chem.* **1968**, *45*, 162–171.
19. Helbert, W.; Chanzy, H. *Starch/Stärke* **1996**, *84*, 185–188.
20. Chanzy, H.; Vuong, R.; Jésior, J. C. *Starch/Stärke* **1990**, *42*, 377–379.
21. Buléon, A.; Pontoire, B.; Riekel, C.; Chanzy, H.; Helbert, W.; Vuong, R. *Macromolecules* **1997**, *30*, 3952–3954.
22. Buléon, A.; Gerard, C.; Riekel, C.; Vuong, R.; Chanzy, H. *Macromolecules* **1998**, *31*, 6605–6610.
23. Gallant, D. J.; Guilbot, A. *Stärke* **1971**, *23*, 244–250.
24. Tamayo, J.; García, R. *Appl. Phys. Lett.* **1997**, *71*, 2394–2396.
25. Cleveland, J. P.; Anczykowski, B.; Scmid, A. E.; Elings, V. B. *Appl. Phys. Lett.* **1998**, *72*, 2613–2615.
26. Raghavan, D.; Gu, X.; Nguyen, T.; VanLandingham, M.; Karim, A. *Macromol.* **2000**, *33*, 2573–2583.
27. Schmitz, I.; Schreiner, M.; Friedbacher, G.; Grasserbauer, M. *Appl. Surf. Sci.* **1997**, *115*, 190–198.
28. Oostergetel, G. T.; van Bruggen, E. F. J. *Carbohydr. Polym.* **1993**, *21*, 7–12.
29. Waigh, T. A.; Perry, P.; Riekel, C.; Gidley, M. J.; Donald, A. M. *Macromol.* **1998**, *31*, 7980–7984.
30. McMaster, T. J.; Hobbs, J. K.; Barham, P. J.; Miles, M. J. *Probe Microsc.* **1997**, *1*, 43–56.
31. T.J. McMaster, PhD thesis, University of Bristol, 1996.
32. James, P. J.; McMaster, T. J.; Newton, J. M.; Miles, M. J. *Polymer* **2000**, *41*, 4223–4231.